JASA ARTICLE

A modal expansion method for simulating reverberant sound fields generated by a directional source in a rectangular enclosure

Jiaxin Zhong,[a] Haishan Zou, and Jing Lu[b]
Key Laboratory of Modern Acoustics and Institute of Acoustics, Nanjing University, Nanjing 210093, China

ABSTRACT:
The prediction of reverberant sound fields generated by a directional source is of great interest because practical sound sources are not omnidirectional, especially at high frequencies. For an arbitrary directional source described by cylindrical and spherical harmonics, this paper developed a modal expansion method for calculating the reverberant sound field generated by such a source in both two-dimensional and three-dimensional rectangular enclosures with finite impedance walls. The key is to express the modal source density using the cylindrical or spherical harmonic expansion coefficients of the directional source. A method based on the fast Fourier transform is proposed to enable the fast computation of the summation of enclosure modes when walls are lightly damped or rigid. This makes it possible to obtain accurate reverberant sound fields even in a large room and/or at high frequencies with a relatively low computational load. Numerical results with several typical directional sources are presented. The efficiency and the accuracy of the proposed method are validated by the comparison to the results obtained using the finite element method. © *2023 Acoustical Society of America*. https://doi.org/10.1121/10.0020070

(Received 8 December 2022; revised 22 May 2023; accepted 20 June 2023; published online 12 July 2023)
[Editor: Ning Xiang] Pages: 203–216

I. INTRODUCTION

The directivity of sound sources has significant effects in many audio applications. For example, active noise control systems consisting of highly directional sources can mitigate the localized noise without adversely affecting other areas.[1,2] Recent advancements in design and implementation of higher-order directional loudspeakers bring more possibilities and flexibilities than omnidirectional ones in sound field reproduction.[3–5] Better auralization performance can be achieved after including the source directivity.[6] The sound field generated by a directional source in free space has been investigated intensively. As most sound sources are used in reverberant environments, such as rooms and automobile cabins, incorporating the source directivity in simulating reverberant sound fields is receiving increasing interest.[7] Although irregularly shaped enclosures are more realistic in practical applications, the rectangular enclosure remains the most commonly simulated acoustic environment due to its simplicity and its ability to facilitate the investigation of reverberant sound field properties.[8–10] The rectangular enclosure also serves as a building block for solving problems involving more complex structures. For instance, solutions of the reverberant sound fields in rectangular enclosures are utilized to calculate the sound field in coupled rectangular enclosures,[11] door slits on ground,[12] baffled openings in walls,[13] rectangular-like enclosures with leaning walls,[14] and so on. The aim of this work is to develop a computationally efficient wave-based method in the frequency domain for calculating the reverberant sound field generated by an arbitrary directional source in a rectangular enclosure.

There are generally two ways to represent a directional source: collections of point monopole sources and multipoles. Representation using a large collection of point monopole sources is based on the fact that any sound field can be approximated by a set of point sources summed together with appropriate amplitudes and phases. By assuming an array of point sources, the source strength (also known as the driving function) for each source is obtained via fitting against a predefined or measured directivity.[15,16] The multipole-based methods express the sound field radiated by a directional source using the cylindrical[4] and spherical[8] harmonic representations in two-dimensional (2D) and three-dimensional (3D) models, respectively. The concept is that the cylindrical or spherical harmonics form an orthogonal and complete basis for any well-behaved functions defined on a circle and a sphere, respectively, so that the directivity can be represented using either basis. This usually allows for a sparse representation of the source directivity compared to point monopole sources. In addition, the sources are also increasingly measured via cylindrical or spherical harmonics,[17] making it prevailing in wave-based simulations.[18]

There are many methods for simulating the reverberant sound fields in rectangular enclosures.[10,19,20] Among them the image source method (ISM) is one of the most popular

[a]Also at: Graduate Program in Acoustics, The Pennsylvania State University, University Park, PA 16802, USA.
[b]Also at: NJU-Horizon Intelligent Audio Lab, Horizon Robotics, Nanjing 210038, China, and Nanjing Institute of Advanced Artificial Intelligence, Nanjing 210014, China. Electronic mail: lujing@nju.edu.cn

methods due to its simplicity. Early studies focus on modeling omnidirectional sources in an enclosure[21] as well as the fast computation algorithms.[22] In 2012, the ISM was generalized for modeling directional sources placed in a 2D rectangular enclosure,[4] and it was further extended for the 3D rectangular enclosure.[8] The key idea is to mirror the cylindrical and spherical harmonic patterns of the directional source so that the multiple reflections due to enclosure walls can be modeled. This provides a convenient way to simulate the reverberant sound fields generated by a directional source and was used in various kinds of applications in simulating binaural room transfer functions,[23] sound source localizations,[24,25] spatial active noise control,[26,27] and sound field reproductions.[28,29]

The ISM provides an exact solution to the wave equation for a rectangular enclosure with rigid walls, but it assumes angle-independent wall reflection coefficients, making it inherently inaccurate for the enclosure with finite impedance walls, especially when the source or receiver is close to the wall.[21] Although the accuracy can be improved by using angle-dependent wall reflection coefficients, it makes the computation much more complicated as these coefficients depend on multiple parameters and involve numerical integrations over angles in the complex plane.[30,31] In addition, the required number of image sources to obtain a satisfactory converged solution scales with the reverberation time.[4] This means that the computation becomes very time-consuming for a lightly damped enclosure that has a large reverberation time. Moreover, the computational cost becomes heavier if there are many receivers in the enclosure.[32] Although the convergence is fast at small reverberation time, the prediction accuracy would be deteriorated if the angle-independent wall reflection coefficients are used.

An alternative to the ISM is the modal expansion method (MEM), which expresses the reverberant sound field as the superposition of a complete set of modal functions (eigenfunctions). The MEM was first used to solve for the reverberant sound field in a rectangular enclosure with rigid or lightly damped walls[33] and then extended to accommodate the finite impedance walls.[9,34] A hybrid MEM was also proposed to combine the free field Green's function and a modal expansion to improve the convergence speed.[35] Although most MEMs are used in the frequency domain, they can also be extended to simulate the transient response.[36] The major advantage of the MEM is that it provides exact solutions to the wave equation with appropriate boundary conditions, so it is in principle more accurate than the ISM when the enclosure has finite impedance walls. For an arbitrary source placed in an enclosure, a key of using MEMs is to obtain the modal source density of this source, which is the inner product of the source density and the modal function.[36] However, the source density for a directional source described by cylindrical or spherical harmonics is usually unknown. Another challenge of using MEMs is that the required number of enclosure modes to obtain converged results scales with the enclosure volume and the frequency cubed. This would limit the applications of MEMs to low frequency responses in small enclosures. This paper proposes to extend the MEM to incorporate the source directivity and develop a computationally efficient algorithm to reduce the computational load.

This paper is organized as follows. The physical model to be investigated and cylindrical and spherical harmonic representations of directional sources are presented in Sec. II. The modal expansion of reverberant sound fields in a rectangular enclosure with finite impedance walls as well as with lightly damped walls is summarized in Sec. III. A fast computation method utilizing the fast Fourier transform (FFT) is developed in Sec. III D, which makes it possible to simulate the reverberant sound fields in a large enclosure and/or at high frequencies with a relatively low computation load. Section IV solves the modal source density for an arbitrary directional source using its cylindrical and spherical harmonic expansion coefficients so that the reverberant sound field generated by such a source can be calculated using the MEM. Finally, simulation results with several typical directional sources are presented in Sec. V and compared against those obtained using the finite element method (FEM).

II. PROBLEM FORMULATION

A. Physical model

Figure 1 shows the physical model to be investigated in this paper. Both 2D (Ref. 4) and 3D (Ref. 8) enclosures are considered for their extensive applications. The 2D and 3D (global) Cartesian coordinate systems Oxy and $Oxyz$ are established with their origin at one corner of the 2D and 3D enclosures, respectively. The dimensions of the 2D and 3D enclosures are $S = L_x \times L_y$ and $V = L_x \times L_y \times L_z$, respectively, and the walls are denoted by ∂S and ∂V.

A directional sound source is placed in the enclosure with its acoustic center at $\boldsymbol{\rho}_c = (x_c, y_c)$ or $\mathbf{r}_c = (x_c, y_c, z_c)$. The sound source is assumed to be spatially confined, so it is represented by a finite extent distributed source inscribed within a circle of radius ρ_0 and a sphere of radius r_0 as shown in Figs. 1(a) and 1(b), respectively. For the method developed in this paper, it is more convenient to define a primed (local) coordinate system $O'x'y'$ in the 2D enclosure ($O'x'y'z'$ in the 3D enclosure) with the positive x' (z' in the 3D enclosure) axis being the direction of the mainlobe and the origin O' at the acoustic center of the source. The radiation directions of the source are denoted by unit vectors $\mathbf{n}_d = (\cos\varphi_d, \sin\varphi_d)$ and $\mathbf{n}_d = (\sin\theta_d\cos\varphi_d, \sin\theta_d\sin\varphi_d, \cos\theta_d)$, in 2D and 3D enclosures, respectively. The angle φ_d is the azimuthal angle in the polar coordinate system (ρ, φ) in the 2D enclosure. The angles θ_d and φ_d correspond to the zenithal and azimuthal angles in the spherical coordinate system (r, θ, φ), respectively, in the 3D enclosure. Throughout this work, a harmonic term $\exp(-i\omega t)$ is assumed, where the angular frequency $\omega = 2\pi f$, f is the frequency, i is the imaginary unit, and t is the time. The objective is to calculate the reverberant sound field generated by

JASA
https://doi.org/10.1121/10.0020070

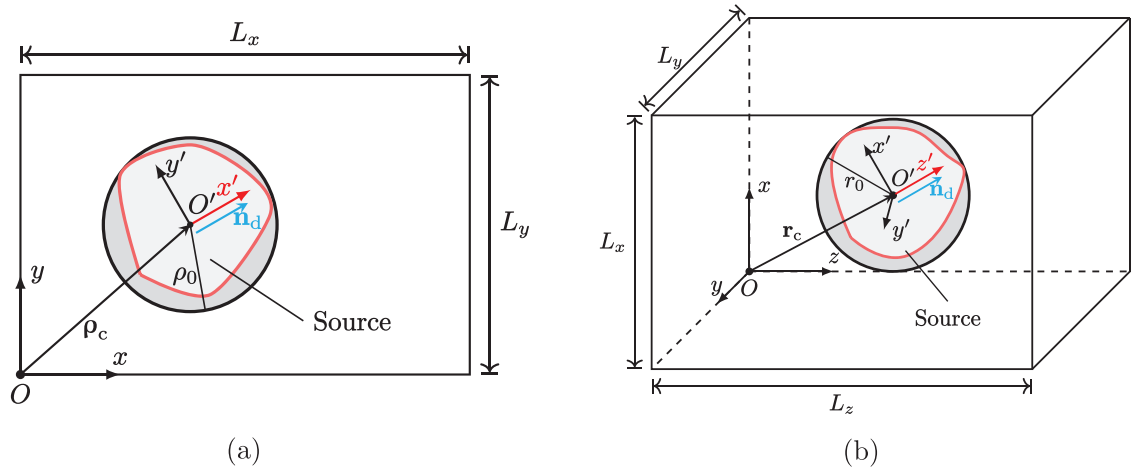

FIG. 1. (Color online) Sketch of a directional source in (a) 2D and (b) 3D rectangular enclosures. The directional source is represented by a finite extent distributed source inscribed within (a) a circle of radius ρ_0 and (b) a sphere of radius r_0.

an arbitrary directional source in a 2D or 3D rectangular enclosure.

B. Cylindrical harmonic representation of a directional source in 2D space

The sound pressure at an exterior field point $\boldsymbol{\rho}'$ generated by an arbitrary directional source in 2D space can be represented by the cylindrical harmonics as[4]

$$p(\boldsymbol{\rho}') = \frac{\rho_{\text{air}}\omega}{4}\sum_{m=-\infty}^{\infty} A_m(k)H_m(k\rho')\mathrm{e}^{\mathrm{i}m\varphi'}, \quad \rho' > \rho_0, \tag{1}$$

where ρ' and φ' are the polar and azimuthal coordinates of the point $\boldsymbol{\rho}'$. The normalization factor $\rho_{\text{air}}\omega/4$ represents the self-radiation resistance of a point monopole source with the wavenumber k in 2D free space, where ρ_{air} is the air density, the wavenumber $k = \omega/c_{\text{air}} + \mathrm{i}\alpha$, c_{air} is the sound speed in air, and α is the attenuation coefficient at the frequency f due to atmospheric absorption.[37] The radius of the circle just enclosing the source is denoted by ρ_0 as shown in Fig. 1(a). In Eq. (1), $H_m(\cdot)$ is the Hankel function of the first kind, and $A_m(k)$ are expansion coefficients that can be obtained by analytical derivations and/or measured results.[38] This directional source can be seen as the radiation from a finite extent distributed source with a source density of $q'(\boldsymbol{\rho}'_{\text{s}})$, so that $q'(\boldsymbol{\rho}'_{\text{s}}) = 0$ for $\rho'_{\text{s}} > \rho_0$. Note that the field (or observation) point $\boldsymbol{\rho}'$ is represented in the primed coordinate system.

In free space, the sound pressure generated by such a distributed source can be obtained by[39]

$$p(\boldsymbol{\rho}') = -\mathrm{i}\rho_{\text{air}}\omega\int\!\!\int_{\rho'_{\text{s}}\le\rho_0} q'(\boldsymbol{\rho}'_{\text{s}})g_{2\text{D}}(\boldsymbol{\rho}' - \boldsymbol{\rho}'_{\text{s}})\mathrm{d}^2\boldsymbol{\rho}'_{\text{s}}, \tag{2}$$

where the 2D Green's function is expressed as

$$g_{2\text{D}}(\boldsymbol{\rho}' - \boldsymbol{\rho}'_{\text{s}}) = \frac{\mathrm{i}}{4}H_0(k|\boldsymbol{\rho}' - \boldsymbol{\rho}'_{\text{s}}|). \tag{3}$$

It is known that $g_{2\text{D}}$ can be represented as the superposition of cylindrical waves by[39,40]

$$g_{2\text{D}}(\boldsymbol{\rho}' - \boldsymbol{\rho}'_{\text{s}}) = \frac{\mathrm{i}}{4}\sum_{m=-\infty}^{\infty} J_m(k\rho'_<)H_m(k\rho'_>)\mathrm{e}^{\mathrm{i}m(\varphi' - \varphi'_{\text{s}})}, \tag{4}$$

where $J_m(\cdot)$ is the Bessel function, $\rho'_< = \min(\rho', \rho'_{\text{s}})$, and $\rho'_> = \max(\rho', \rho'_{\text{s}})$. The substitution of Eq. (4) into Eq. (2) yields

$$p(\boldsymbol{\rho}') = \frac{\rho_{\text{air}}\omega}{4}\sum_{m=-\infty}^{\infty}\left[\int\!\!\int_{\rho'_{\text{s}}\le\rho_0} q'(\boldsymbol{\rho}'_{\text{s}})J_m(k\rho'_{\text{s}})\mathrm{e}^{-\mathrm{i}m\varphi'_{\text{s}}}\mathrm{d}^2\boldsymbol{\rho}'_{\text{s}}\right] \times H_m(k\rho')\mathrm{e}^{\mathrm{i}m\varphi'}. \tag{5}$$

By comparing Eqs. (5) and (1), it can be found that the cylindrical harmonic expansion coefficients $A_m(k)$ and the source density $q'(\boldsymbol{\rho}'_{\text{s}})$ are related by

$$A_m(k) = \int\!\!\int_{\rho'_{\text{s}}\le\rho_0} q'(\boldsymbol{\rho}'_{\text{s}})J_m(k\rho'_{\text{s}})\mathrm{e}^{-\mathrm{i}m\varphi'_{\text{s}}}\mathrm{d}^2\boldsymbol{\rho}'_{\text{s}}. \tag{6}$$

Equation (6) shows that an arbitrary directional source described by Eq. (1) can be seen as the radiation from an equivalent source with a source density of $q'(\boldsymbol{\rho}'_{\text{s}})$ inside the circle $\rho' \le \rho_0$.

C. Spherical harmonic representation of a directional source in 3D space

The sound pressure at an exterior field point $\mathbf{r}'$ generated by a directional source in 3D space can be represented by the spherical harmonics as[8,41,42]

$$p(\mathbf{r}') = \frac{\rho_{\text{air}}\omega k}{4\pi}\sum_{\ell=0}^{\infty}\sum_{m=-\ell}^{\ell} A_\ell^m(k)\mathrm{h}_\ell(kr')Y_\ell^m(\theta', \varphi'), \tag{7}$$

where r', θ', and φ' are, respectively, the radial, zenithal, and azimuthal coordinates of the point $\mathbf{r}'$, the normalization factor $\rho_{\text{air}}\omega k/(4\pi)$ represents the self-radiation resistance of a point monopole source with the wavenumber k in 3D free space, $\mathrm{h}_\ell(\cdot)$ is the spherical Hankel function of the first kind,

$Y_\ell^m(\cdot,\cdot)$ is the spherical harmonics of degree l and order m, and $A_\ell^m(k)$ are expansion coefficients. Similar to the 2D model, this directional source can be seen as the radiation from a finite extent distributed source with a source density of $q'(\mathbf{r}'_s)$, so that $q'(\mathbf{r}'_s) = 0$ for $r'_s > r_0$. Note that the field (or observation) point $\mathbf{r}'$ is represented in the primed coordinate system.

In free space, the sound pressure generated by such a distributed source can be obtained by

$$p(\mathbf{r}') = -\mathrm{i}\rho_{\mathrm{air}}\omega \iiint_{r'_s \le r_0} q'(\mathbf{r}'_s) g_{3D}(\mathbf{r}' - \mathbf{r}'_s)\mathrm{d}^3\mathbf{r}'_s, \tag{8}$$

where the 3D Green's function is expressed as

$$g_{3D}(\mathbf{r}' - \mathbf{r}'_s) = \frac{\mathrm{e}^{\mathrm{i}k|\mathbf{r}'-\mathbf{r}'_s|}}{4\pi|\mathbf{r}' - \mathbf{r}'_s|}. \tag{9}$$

It is known that g_{3D} can be represented as the superposition of spherical waves by[43]

$$g_{3D}(\mathbf{r}' - \mathbf{r}'_s) = \mathrm{i}k \sum_{\ell=0}^{\infty} \mathrm{j}_\ell(kr'_<)\mathrm{h}_\ell(kr'_>) \times \sum_{m=-\ell}^{\ell} Y_\ell^m(\theta', \varphi') Y_\ell^{m,*}(\theta'_s, \varphi'_s), \tag{10}$$

where the superscript "*" represents the complex conjugation, $\mathrm{j}_\ell(\cdot)$ is the spherical Bessel function of the first kind, $r'_< = \min(r', r'_s)$, and $r'_> = \max(r', r'_s)$. The substitution of Eq. (10) into Eq. (8) yields

$$p(\mathbf{r}') = \rho_{\mathrm{air}}\omega k \sum_{\ell=0}^{\infty} \sum_{m=-\ell}^{\ell} \left[\iiint_{r'_s \le r_0} q'(\mathbf{r}'_s)\mathrm{j}_\ell(kr'_s) \times Y_\ell^{m,*}(\theta'_s, \varphi'_s)\mathrm{d}^3\mathbf{r}'_s \right] \mathrm{h}_\ell(kr')Y_\ell^m(\theta', \varphi'). \tag{11}$$

By comparing Eqs. (11) and (7), it is observed that the spherical expansion coefficients $A_\ell^m(k)$ and the source density $q'(\mathbf{r}'_s)$ are related by

$$A_\ell^m(k) = 4\pi \iiint_{r'_s \le r_0} q(\mathbf{r}'_s)\mathrm{j}_\ell(kr'_s)Y_\ell^{m,*}(\theta'_s, \varphi'_s)\mathrm{d}^3\mathbf{r}'_s. \tag{12}$$

Equation (12) shows that an arbitrary directional source described by Eq. (7) can be seen as the radiation from an equivalent source with a source density of $q'(\mathbf{r}'_s)$ inside the sphere $\mathbf{r}' \le r_0$. The following text aims to develop the modal expansion for calculating the reverberant sound field generated by a directional source described by Eq. (1) or (7).

III. MODAL EXPANSION OF NON-DIFFUSE REVERBERANT SOUND FIELDS

The framework of the modal expansion of reverberant sound fields in a rectangular enclosure is summarized first in Sec. III A. Then the eigenvalues and eigenfunctions involved in the modal expansion are presented for an enclosure with finite impedance and lightly damped walls in Secs. III B and III C, respectively. Finally, in Sec. III D, a computationally efficient method is proposed to enable the fast computation of the summation of modes by using the FFT when the walls are lightly damped. Without loss of generality, the formulas are derived in the 3D model, and the extension of them to the 2D model is straightforward.

A. Framework of the formulation

For an arbitrary source with a source density of $q(\mathbf{r})$, the sound pressure in a rectangular enclosure can be obtained by using the modal expansion as[9]

$$p(\mathbf{r}) = \mathrm{i}\rho_{\mathrm{air}}\omega \sum_{n_x=0}^{\infty} \sum_{n_y=0}^{\infty} \sum_{n_z=0}^{\infty} \frac{Q_n \psi_n(\mathbf{r})}{\Lambda_n(k^2 - k_n^2)}, \tag{13}$$

where $\psi_n(\mathbf{r})$ are eigenfunctions satisfying appropriate boundary conditions on walls. The modal number n denotes the index set of n_x, n_y, and n_z, and the modal wavenumber vector consisting of the corresponding eigenvalues is $\mathbf{k}_n = (k_{n_x}, k_{n_y}, k_{n_z})$ with $k_n^2 = k_{n_x}^2 + k_{n_y}^2 + k_{n_z}^2$. It is noted that all physical quantities in Eq. (13) are expressed in the unprimed coordinate system. The eigenfunctions are orthogonal in the sense that

$$\iiint_V \psi_n(\mathbf{r})\psi_{n'}(\mathbf{r})\mathrm{d}^3\mathbf{r} = \Lambda_n \delta_{nn'}, \tag{14}$$

where $\delta_{nn'}$ is the Kronecker delta function, which equals 1 when $n = n'$ and 0 otherwise. Note that in Eq. (14), $\psi_n(\mathbf{r})$ should be multiplied by $\psi_{n'}(\mathbf{r})$ instead of its complex conjugation.[9,44] The normalization factor is then obtained as

$$\Lambda_n \equiv \iiint_V \psi_n^2(\mathbf{r})\mathrm{d}^3\mathbf{r}. \tag{15}$$

The modal source density in Eq. (13) has the form of

$$Q_n \equiv \iiint_V q(\mathbf{r}_s)\psi_n(\mathbf{r}_s)\mathrm{d}^3\mathbf{r}_s, \tag{16}$$

which can be seen as the inner product of the source density $q(\mathbf{r}_s)$ and the modal function $\psi_n(\mathbf{r}_s)$. Note that $q(\mathbf{r}_s)$ is the source density defined in the unprimed coordinate system, which differs from $q'(\mathbf{r}'_s)$ defined in the primed coordinate system. The difficulty of modeling a directional source in an enclosure is that the source density is usually unknown so that the modal source density is unable to be calculated using Eq. (16).

B. Finite impedance walls

Suppose the walls of the enclosure have a finite specific acoustic impedance of $Z(\mathbf{r})$, and define the normalized specific acoustic admittance as $\beta(\mathbf{r}) = \rho_{\mathrm{air}}c_{\mathrm{air}}/Z(\mathbf{r})$. This definition is chosen because it is convenient to represent a

https://doi.org/10.1121/10.0020070

commonly occurring case when the wall is rigid, i.e., $\beta = 0$. The boundary conditions for eigenfunctions then read[9]

$$\mathbf{n} \cdot \nabla \psi_n(\mathbf{r}) = \mathrm{i}\beta(\mathbf{r}) k \psi_n(\mathbf{r}), \quad \mathbf{r} \in \partial V, \tag{17}$$

where the vector $\mathbf{n}$ is the unit normal vector of ∂V, which points outward from the enclosure walls. Note that Eq. (17) differs by a factor of –1 from that used in some literature, because this paper adopts the time-harmonic convention of $\exp(-\mathrm{i}\omega t)$ instead of $\exp(\mathrm{i}\omega t)$. The reason for this preference can be found in Ref. 45. It is worth noting that the normalized specific acoustic admittance can vary with frequency by utilizing a frequency-dependent specific acoustic impedance $Z(\mathbf{r}, \omega)$. In contrast, the ISM often assumes that the wall admittance is proportional to cosine of the incident angle, leading to an angle-independent reflection coefficient.[21] Therefore, when dealing with enclosures that have walls with finite impedance, the MEM developed in this work offers higher accuracy compared to the ISM.

For simplicity, the normalized specific acoustic admittance is assumed to be uniform on each wall and frequency-independent in this work, and $\beta_{\xi,0}$ and β_{ξ,L_ξ} denote the value on the wall $\xi = 0$ and $\xi = L_\xi$, respectively, where $\xi = x, y, z$.

For finite impedance walls, the eigenfunctions can be chosen as[9]

$$\psi_n(\mathbf{r}) = \cos(k_{n_x} x + \gamma_{n_x}) \cos(k_{n_y} y + \gamma_{n_y}) \cos(k_{n_z} z + \gamma_{n_z}), \tag{18}$$

where the modal phases $\boldsymbol{\gamma}_n = (\gamma_{n_x}, \gamma_{n_y}, \gamma_{n_z})$ are determined by the equation

$$k_{n_\xi} \tan \gamma_{n_\xi} = \mathrm{i} k \beta_{\xi,0}, \tag{19}$$

and the eigenvalues k_{n_ξ} are obtained by solving the transcendental equation,[9]

$$(k^2 \beta_{\xi,0} \beta_{\xi,L_\xi} + k_{n_\xi}^2) \tan(k_{n_\xi} L_\xi) = -\mathrm{i} k k_{n_\xi} (\beta_{\xi,0} + \beta_{\xi,L_\xi}), \tag{20}$$

which are complex numbers in general. The normalization factor given by Eq. (15) is then obtained by directly evaluating the integral as

$$\Lambda_n = \frac{V}{8} \prod_{\xi=x,y,z} \left[1 + \mathrm{sinc}(k_{n_\xi} L_\xi) \cos(k_{n_\xi} L_\xi + 2\gamma_{n_\xi})\right], \tag{21}$$

where the volume $V = L_x L_y L_z$ and $\mathrm{sinc} x \equiv (\sin x)/x$ is the sinc function.

C. Lightly damped or rigid walls

For lightly damped or rigid walls, the formulation can be further simplified. The boundary conditions for rigid walls are obtained by setting $\beta = 0$ in Eq. (17). The eigenvalues are known to be

$$k_{n_\xi} = \frac{n_\xi \pi}{L_\xi}, \tag{22}$$

and the corresponding eigenfunctions are

$$\psi_n(\mathbf{r}) = \cos(k_{n_x} x) \cos(k_{n_y} y) \cos(k_{n_z} z), \tag{23}$$

which can be seen as a reduced form of Eq. (18) by setting $\gamma_{n_\xi} = 0$ into it. The normalization factor Λ_n given by Eq. (15) reduces to S/ε_n and V/ε_n for 2D and 3D models, respectively, where $\varepsilon_n = \varepsilon_{n_x} \varepsilon_{n_y} \varepsilon_{n_z}$ and the Neumann factor $\varepsilon_{n_\xi} = 1$ when $n_\xi = 0$, $\varepsilon_{n_\xi} = 2$ when $n_\xi \neq 0$.

For lightly damped walls with $0 < |\beta| \ll 1$, the eigenvalues and eigenfunctions remain the same as given by Eqs. (22) and (23). However, the wavenumber $k = \omega/c_0 + \mathrm{i}\alpha$ is modified as $k = \omega/c_0 + \mathrm{i}(\alpha + D_n/2)$ to include the damping effects, where D_n is the damping term of each mode[36,46]

$$D_n \equiv \frac{1}{\Lambda_n} \int\int_{\partial V} \beta(\mathbf{r}) \psi_n^2(\mathbf{r}) \mathrm{d}^2 \mathbf{r}. \tag{24}$$

Based on the assumption that $\beta(\mathbf{r})$ is uniform on each wall, it is obtained that

$$D_n = \frac{1}{V} \Big[\varepsilon_{n_x} S_x (\beta_{x,0} + \beta_{x,L_x}) + \varepsilon_{n_y} S_y (\beta_{y,0} + \beta_{y,L_y}) + \varepsilon_{n_z} S_z (\beta_{z,0} + \beta_{z,L_z})\Big], \tag{25}$$

where $S_x = L_y L_z$, $S_y = L_x L_z$, and $S_z = L_x L_y$ are the areas of the wall perpendicular to x, y, and z axes, respectively.

D. Fast computation using FFT

In numerical computations, the leading terms of the modal expansion given by Eq. (13) need to be truncated to obtain a converged result. Let us assume that the truncation terms are $N_x/2$, $N_y/2$, and $N_z/2$ for n_x, n_y, and n_z, respectively. Meanwhile, by using the relation $\cos(k_{n_\xi} \xi) = (\mathrm{e}^{\mathrm{i} k_{n_\xi} \xi} + \mathrm{e}^{-\mathrm{i} k_{n_\xi} \xi})/2$, Eq. (13) can be rewritten as

$$p(\mathbf{r}) \approx \sum_{n_x=-N_x/2}^{N_x/2-1} \sum_{n_y=-N_y/2}^{N_y/2-1} \sum_{n_z=-N_z/2}^{N_z/2-1} \tilde{p}(\mathbf{k}_n) \mathrm{e}^{\mathrm{i}\mathbf{k}_n \cdot \mathbf{r}} \tag{26}$$

for lightly damped enclosures, where $\mathbf{k}_n = (n_x \Delta k_x, n_y \Delta k_y, n_z \Delta k_z)$, $\Delta k_\xi = \pi/L_\xi$, $\xi = x, y, z$, and $\tilde{p}(\mathbf{k}_n)$ is defined as

$$\tilde{p}(\mathbf{k}_n) \equiv \frac{\mathrm{i}\rho_{\mathrm{air}} \omega Q_n}{V(k^2 - k_n^2)}. \tag{27}$$

If the sound pressure at the grid points $\mathbf{r}_m = (m_x \Delta x, m_y \Delta y, m_z \Delta z)$ are evaluated, Eq. (26) can be straightforwardly transformed into the form of 3D inverse discrete Fourier transform with respect to $\tilde{p}(\mathbf{k}_n)$, where $\Delta\xi \equiv 2L_\xi/N_\xi$, $m_\xi = -N_\xi/2, -N_\xi/2+1, \ldots, N_\xi/2-1$, and $\xi = x, y, z$. Therefore, it can be efficiently computed utilizing the FFT. The reader is referred to Sec. 1.8.2 of Ref. 41 for more details. The direct calculation of Eq. (26) requires the order of $N_x^2 N_y^2 N_z^2$ multiplications and additions to obtain the reverberant sound field. However, the complexity of the computation with FFT reduces to only $N_x N_y N_z (\log N_x)(\log N_y)(\log N_z)$ without loss of accuracy. It is then much more

efficient, especially at high frequencies and/or in large enclosures.

It is noted that the computation of Eq. (26) using FFT is valid only for lightly damped walls when $\mathbf{k}_n$ are real valued as given by Eq. (22). Nevertheless, the computation using FFT still significantly reduces the computation load unless walls have finite impedance in all directions. For example, when the enclosure walls are nonrigid only in the z direction,[9,10,13] the computation efficiency can still be improved by using the FFT in both x and y directions. Furthermore, the fast computation facilitated by the proposed FFT method in this work also holds great potential for simulating various other acoustic applications, where modal summations for rigid walls are required. These applications include simulating the sound field in coupled rectangular enclosures,[11] door slits on ground,[12] baffled openings in walls,[13] rectangular-like enclosures with leaning walls,[14] and so on.

IV. MODAL SOURCE DENSITY FOR DIRECTIONAL SOURCES

It can be found in Sec. III that the reverberant sound field in an enclosure can be obtained using the modal expansion given by Eq. (13) once the modal source density given by Eq. (16) is known. However, the source density $q(\mathbf{r}_s)$ is generally unknown for a given directional source described by Eqs. (1) and (7). It will be shown in Secs. IV A and IV B that the modal source density can be obtained in terms of the cylindrical and spherical harmonic expansion coefficients in an indirect way for both 2D and 3D models.

A. 2D directional sources

To obtain the modal source density for a 2D directional source, an auxiliary integral is introduced as

$$I(\mathbf{k}_n) = \int\int_S q(\boldsymbol{\rho}_s) e^{-i\mathbf{k}_n\cdot\boldsymbol{\rho}_s} d^2\boldsymbol{\rho}_s. \tag{28}$$

It can be shown that the modal source density given by Eq. (16) is

$$Q_n = \frac{1}{4}\sum_{\pm} e^{-i(\gamma_{n_x}+\gamma_{n_y})} I(\pm k_{n_x}, \pm k_{n_y}), \tag{29}$$

where the symbol $\sum_{\pm}$ denotes the summation of four possible combinations of positive and negative signs. Consequently, once the integral given by Eq. (28) is determined, the modal source density is obtained according to Eq. (29). Our approach is to solve the integral by using the cylindrical harmonic expansion coefficients represented by Eq. (6).

It is noted that the source density $q(\boldsymbol{\rho}_s)$ in Eq. (28) is given in the unprimed coordinate system Oxy, the origin of which is coincident with a corner of the enclosure. In most cases, the source density is more conveniently represented in a primed coordinate system $O'x'y'$ with the origin at the acoustic center of the source and the positive x' axis in the direction of $\mathbf{n}_d = (\cos\varphi_d, \sin\varphi_d)$, which is the center of the mainlobe of the source. The primed axes $x'y'$ can be seen as rotating the unprimed ones xy through an angle φ_d followed by a translation of $\boldsymbol{\rho}_c$. The coordinates of the source point in the primed system $\boldsymbol{\rho}'_s$ and the coordinates in the unprimed one $\boldsymbol{\rho}_s$ are then related by

$$\boldsymbol{\rho}'_s = \mathbf{R}(\boldsymbol{\rho}_s - \boldsymbol{\rho}_c), \tag{30}$$

where the rotation matrix is

$$\mathbf{R} = \begin{bmatrix} \cos\varphi_d & \sin\varphi_d \\ -\sin\varphi_d & \cos\varphi_d \end{bmatrix}. \tag{31}$$

By changing the integration region in Eq. (28) from S to $\rho'_s \le \rho_0$, it is obtained that

$$I(\mathbf{k}_n) = \int\int_{\rho'_s\le\rho_0} q'(\boldsymbol{\rho}'_s) e^{-i\mathbf{k}_n\cdot\boldsymbol{\rho}_s} d^2\boldsymbol{\rho}'_s, \tag{32}$$

where the relation $d^2\boldsymbol{\rho}'_s = d^2\boldsymbol{\rho}_s$ has been used because the determinant of the rotation matrix is unit. Note that the source point $\boldsymbol{\rho}_s$ in the exponential function is still expressed in the unprimed coordinate system. Because $\mathbf{R}$ is orthonormal, $\mathbf{R}^{-1} = \mathbf{R}^T$, where $\mathbf{R}^{-1}$ is the inverse matrix of $\mathbf{R}$, and the superscript "T" denotes the transpose. The inverse transformation from $\boldsymbol{\rho}'_s$ to $\boldsymbol{\rho}_s$ is obtained by $\boldsymbol{\rho}_s = \mathbf{R}^{-1}\boldsymbol{\rho}'_s + \boldsymbol{\rho}_c = \mathbf{R}^T\boldsymbol{\rho}'_s + \boldsymbol{\rho}_c$. The phase term in Eq. (32), i.e., $\mathbf{k}_n\cdot\boldsymbol{\rho}_s$, can be written as $\mathbf{k}_n^T\boldsymbol{\rho}_s$ when $\mathbf{k}_n$ and $\boldsymbol{\rho}_s$ are represented as column vectors. Accordingly, $\mathbf{k}_n^T\boldsymbol{\rho}_s = \mathbf{k}_n^T(\mathbf{R}^T\boldsymbol{\rho}'_s + \boldsymbol{\rho}_c) = (\mathbf{R}\mathbf{k}_n)^T\boldsymbol{\rho}'_s + \mathbf{k}_n^T\boldsymbol{\rho}_c$, which can also be written as $(\mathbf{R}\mathbf{k}_n)\cdot\boldsymbol{\rho}'_s + \mathbf{k}_n\cdot\boldsymbol{\rho}_c$ using the inner product notation. Then

$$I(\mathbf{k}_n) = e^{-i\mathbf{k}_n\cdot\boldsymbol{\rho}_c}\int\int_{\rho'_s\le\rho_0} q'(\boldsymbol{\rho}'_s) e^{-i\mathbf{k}'_n\cdot\boldsymbol{\rho}'_s} d^2\boldsymbol{\rho}'_s, \tag{33}$$

where a primed modal wavenumber vector is defined as $\mathbf{k}'_n = \mathbf{R}\mathbf{k}_n$. It is clear that $k'_n \equiv |\mathbf{k}'_n| = |\mathbf{k}_n| = k_n$.

It is known that the cylindrical expansion holds that

$$e^{-i\mathbf{k}'_n\cdot\boldsymbol{\rho}'_s} = \sum_{m=-\infty}^{\infty} i^{-m} J_m(k_n\rho'_s) e^{im(\varphi_{k'_n} - \varphi'_s)}, \tag{34}$$

where $(k_n, \varphi_{k'_n})$ are the polar coordinates of $\mathbf{k}'_n$ such that $\varphi_{k'_n} = \tan^{-1}(k'_{n_y}/k'_{n_x})$. Equation (34) represents the cylindrical expansion of a plane wave arriving from the direction $-\mathbf{k}'_n$ when $\mathbf{k}'_n$ are real valued. The substitution of Eq. (34) into Eq. (33) yields

$$I(\mathbf{k}_n) = e^{-i\mathbf{k}_n\cdot\boldsymbol{\rho}_c}\sum_{m=-\infty}^{\infty} i^{-m} e^{im\varphi_{k'_n}} \times \int\int_{\rho'_s\le\rho_0} q'(\boldsymbol{\rho}'_s) J_m(k_n\rho'_s) e^{-im\varphi'_s} d^2\boldsymbol{\rho}'_s. \tag{35}$$

By comparing Eqs. (35) and (6), it can be found that

$$I(\mathbf{k}_n) = e^{-i\mathbf{k}_n\cdot\boldsymbol{\rho}_c}\sum_{m=-\infty}^{\infty} i^{-m} A_m(k_n) e^{im\varphi_{k'_n}}. \tag{36}$$

https://doi.org/10.1121/10.0020070

Equation (36) is one of main results of this paper. Consider an arbitrary directional source, the sound field generated by which can be represented using the cylindrical harmonics as shown by Eq. (1). The radiation from such as a source can be seen as that from an equivalent distributed source with a source density of $q'(\boldsymbol{\rho}'_s)$ spatially confined in a circle with a radius of ρ_0. Once the expansion coefficients $A_m(k)$ are determined by analytical and/or experimental methods, the auxiliary integral $I(\mathbf{k}_n)$ can be obtained using Eq. (36), where the modal eigenvalues $\mathbf{k}_n$ are obtained using Eq. (20) or (22) and the rotated modal eigenvalues $\mathbf{k}'_n = \mathbf{R}\mathbf{k}_n$ with the rotation matrix given by Eq. (31). Then the modal source density for this directional source is obtained by Eq. (29), where the phase term (if needed) γ_{n_ξ} is obtained using Eq. (19). Finally, the reverberant sound field in an enclosure is calculated using Eq. (13) with the eigenfunctions given by Eq. (18) or (23). In conclusion, the modal source density Q_n is indirectly obtained using the cylindrical harmonic expansion coefficients $A_m(k)$.

It is noted that the integral in Eq. (33) represents a 2D spatial Fourier transform of the primed source density $q'(\boldsymbol{\rho}'_s)$, which reads

$$\tilde{q}'(\mathbf{k}'_n) \equiv \int\int_{\rho'_s \le \rho_0} q'(\boldsymbol{\rho}'_s) e^{-i\mathbf{k}'_n \cdot \boldsymbol{\rho}'_s} d^2\boldsymbol{\rho}'_s. \tag{37}$$

This observation allows for a faster computation of the auxiliary integral than that given by Eq. (36), i.e., $I(\mathbf{k}_n) = e^{-i\mathbf{k}_n \cdot \boldsymbol{\rho}_c} \tilde{q}'(\mathbf{k}'_n)$, when $\tilde{q}'(\mathbf{k}'_n)$ is known for a directional source.

B. 3D directional sources

Similar to Eq. (28), an auxiliary integral is defined as

$$I(\mathbf{k}_n) = \int\int\int_V q(\mathbf{r}_s) e^{-i\mathbf{k}_n \cdot \mathbf{r}_s} d^3\mathbf{r}_s. \tag{38}$$

It can be shown that the modal source density given by Eq. (16) is

$$Q_n = \frac{1}{8} \sum_{\pm} e^{-i(\gamma_{n_x} + \gamma_{n_y} + \gamma_{n_z})} I(\pm k_{n_x}, \pm k_{n_y}, \pm k_{n_z}; \pm\gamma_{n_x}, \pm\gamma_{n_y}, \pm\gamma_{n_z}), \tag{39}$$

where the symbol $\sum_{\pm}$ denotes the summation of eight possible combinations of positive and negative signs.

The primed axes $x'y'z'$ in Fig. 1(b) can be seen as rotating the unprimed axes xyz through an angle pair (θ_d, φ_d) followed by a translation of $\mathbf{r}_c$. The coordinates of a point in the primed system $\mathbf{r}' = (x', y', z')$ and the coordinates in the unprimed one $\mathbf{r} = (x, y, z)$ are then related by

$$\mathbf{r}' = \mathbf{R}(\mathbf{r} - \mathbf{r}_c), \tag{40}$$

where the rotation matrix is obtained by two elementary rotations $\mathbf{R}_y$ and $\mathbf{R}_z$ as

$$\mathbf{R} = \mathbf{R}_y(-\theta_d)\mathbf{R}_z(-\varphi_d) = \begin{bmatrix} \cos\theta_d & 0 & -\sin\theta_d \\ 0 & 1 & 0 \\ \sin\theta_d & 0 & \cos\theta_d \end{bmatrix} \begin{bmatrix} \cos\varphi_d & \sin\varphi_d & 0 \\ -\sin\varphi_d & \cos\varphi_d & 0 \\ 0 & 0 & 1 \end{bmatrix}. \tag{41}$$

By using the relation of Eq. (40), it is obtained that $\mathbf{k}_n \cdot \mathbf{r}_s = \mathbf{k}_n \cdot (\mathbf{R}^{-1}\mathbf{r}'_s + \mathbf{r}_c) = (\mathbf{R}\mathbf{k}_n) \cdot \mathbf{r}'_s + \mathbf{k}_n \cdot \mathbf{r}_c$. By defining the primed wavenumber vector as the rotation of the unprimed one, i.e., $\mathbf{k}'_n = \mathbf{R}\mathbf{k}_n$, the auxiliary integral can be rewritten as

$$I(\mathbf{k}_n) = e^{-i\mathbf{k}_n \cdot \mathbf{r}_c} \int\int\int_{r'_s \le r_0} q'(\mathbf{r}'_s) e^{-i\mathbf{k}'_n \cdot \mathbf{r}'_s} d^3\mathbf{r}'_s. \tag{42}$$

It is known that the spherical harmonic expansion holds that[18]

$$e^{-i\mathbf{k}'_n \cdot \mathbf{r}'_s} = 4\pi \sum_{\ell=0}^{\infty} i^{-\ell} j_\ell(k_n r'_s) \sum_{m=-\ell}^{\ell} Y_\ell^m(\theta_{k'_n}, \varphi_{k'_n}) Y_\ell^{m,*}(\theta'_s, \varphi'_s), \tag{43}$$

where $(k_n, \theta_{k'_n}, \varphi_{k'_n})$ are the spherical coordinates of $\mathbf{k}'_n$. Equation (43) represents the spherical harmonic expansion of a plane wave arriving from the direction $-\mathbf{k}'_n$ when $\mathbf{k}'_n$ are real valued. The substitution of Eq. (43) into Eq. (42) yields

$$I(\mathbf{k}_n) = 4\pi e^{-i\mathbf{k}_n \cdot \mathbf{r}_c} \sum_{\ell=0}^{\infty} \sum_{m=-\ell}^{\ell} i^{-\ell} Y_\ell^m(\theta_{k'_n}, \varphi_{k'_n}) \times \int\int\int_{r'_s \le r_0} q'(\mathbf{r}'_s) j_\ell(k_n r'_s) Y_\ell^{m,*}(\theta'_s, \varphi'_s) d^3\mathbf{r}'_s. \tag{44}$$

By comparing Eqs. (44) and (12), it is observed that

$$I(\mathbf{k}_n) = e^{-i\mathbf{k}_n \cdot \mathbf{r}_c} \sum_{\ell=0}^{\infty} \sum_{m=-\ell}^{\ell} i^{-\ell} A_\ell^m(k_n) Y_\ell^m(\theta_{k'_n}, \varphi_{k'_n}). \tag{45}$$

Equation (45) is one of main results of this paper and is the 3D version of Eq. (36). Consider an arbitrary directional source, the sound field generated by which can be represented using the spherical harmonics as shown by Eq. (7). The radiation from such a source can be seen as that from an equivalent distributed source with a source density of $q'(\mathbf{r}'_s)$ spatially confined in a sphere with a radius of r_0. The calculation process of the modal source density is similar to the 2D model as described below Eq. (36).

It is noted that the integral in Eq. (42) represents a 3D spatial Fourier transform of the primed source density $q'(\mathbf{r}'_s)$, which reads

$$\tilde{q}'(\mathbf{k}'_n) \equiv \int\int\int_{r'_s \le r_0} q'(\mathbf{r}'_s) e^{-i\mathbf{k}'_n \cdot \mathbf{r}'_s} d^3\mathbf{r}'_s. \tag{46}$$

This observation allows for a faster computation of the auxiliary integral than that given by Eq. (45), i.e., $I(\mathbf{k}_n) = e^{-i\mathbf{k}_n \cdot \mathbf{r}_c} \tilde{q}'(\mathbf{k}'_n)$, when $\tilde{q}'(\mathbf{k}'_n)$ is known for a directional source.

V. SIMULATION RESULTS

In the following simulations, the dimensions of the 2D and 3D enclosures are $L_x \times L_y = 1.414 \times 1.156\,\mathrm{m}^2$ and $L_x \times L_y \times L_z = 1.414 \times 1.156 \times 1.5\,\mathrm{m}^3$, respectively. The normalized acoustic specific admittance of the finite impedance wall considered in the simulations is assumed to be $\beta = 0.5$, which corresponds to an absorption coefficient of 0.89.[9] In all cases, three configurations of the enclosure are considered: (i) all walls are rigid, i.e., $\beta = 0$; (ii) the wall on the plane $x = L_x$ is absorptive with a normalized acoustic specific admittance of $\beta = 0.5$ while other walls are rigid; (iii) the wall on the plane $y = 0$ is absorptive with $\beta = 0$ while other walls are rigid. The eigenvalues determined by Eq. (20) are numerically evaluated using the built-in function "FindRoot" in Wolfram Mathematica 13.0, although there are more efficient ways.[9,44] The total surface/volume velocity of the source is set as $Q_0 = 2 \times 10^{-5}\mathrm{m}^2/\mathrm{s}$ and $Q_0 = 2 \times 10^{-5}\mathrm{m}^3/\mathrm{s}$ in 2D and 3D models, respectively. The sound pressure level (SPL) is presented in all following figures with a reference pressure of $2 \times 10^{-5}\mathrm{Pa}$. All calculations with FEM were performed using the commercial software COMSOL Multiphysics 6.0. To ensure converged results in the FEM, the maximal element size is set to be one-tenth of the wavelength, and regular triangular/tetrahedral meshes are used.

The reverberant sound fields generated by a directional source in 2D and 3D enclosures are presented in Secs. V A and V B, respectively. In both sections, the reverberant sound fields at a low frequency are presented first. Then the fields at an extremely high frequency (40 kHz) are presented to investigate the wave propagation of a highly directional source in an enclosure, as well as to show the computational efficiency of the proposed method. The choice of the frequency at 40 kHz results from the application of a highly directional source, i.e., the parametric array loudspeaker (PAL), where the directional audio beam is generated by the nonlinear interactions of intensive ultrasound around 40 kHz.[2] The accurate ultrasound field around 40 kHz is required at first to obtain the audio sound field generated by the PAL. Although the reverberant sound field at such a high frequency is able to be approximately predicted using various kinds of geometric acoustics models,[20] the phase information is neglected or inaccurate so that they cannot be used for the calculations involved in the PAL. The attenuation coefficient due to atmospheric absorption is set as $\alpha = 0.15\mathrm{Np/m}$ at 40 kHz, which is evaluated according to ISO 9613 with a relative humidity of 70% and temperature 20 °C.[37]

A. Directional sources in a 2D enclosure

1. Point monopole source array

Supposing an array consisting of N_s point monopole sources with the ith source located at $\boldsymbol{\rho}'_{s,i} = (\rho'_{s,i}, \varphi'_{s,i})$ described under the primed coordinates system, the source density can be described as $q'(\boldsymbol{\rho}'_s) = \sum_{i=1}^{N_s} Q_{s,i}\delta(\boldsymbol{\rho}'_s - \boldsymbol{\rho}'_{s,i})$, where $\delta(\cdot)$ is the Dirac delta function and $Q_{s,i}$ is the source strength of the ith source. The cylindrical harmonic expansion coefficients can be obtained by using Eqs. (1) and (4) as

$$A_m(k) = \sum_{i=1}^{N_s} Q_{s,i} J_m(k\rho'_{s,i}) \mathrm{e}^{-im\varphi'_{s,i}}. \tag{47}$$

The 2D spatial Fourier transform of the source density is

$$\tilde{q}'(\mathbf{k}'_n) = \sum_{i=1}^{N_s} Q_{s,i} \mathrm{e}^{-i\mathbf{k}'_n \cdot \boldsymbol{\rho}'_{s,i}}. \tag{48}$$

In this subsection, a simple directional source that generates a dipole outgoing sound field is considered first. The dipole is approximated by two point monopole sources located at $(L_x/2 - 0.05\,\mathrm{m}, L_y/2)$ and $(L_x/2 + 0.05\,\mathrm{m}, L_y/2)$ with source strengths of $-Q_0$ and Q_0. Figure 2 compares the reverberant sound fields obtained using the proposed method at 191 Hz, which is the 1,1 mode defined for an enclosure with rigid walls. A dipole radiation pattern can be clearly identified in the left column of Fig. 2. When the wall is set to be absorptive on $x = L_x$ and $y = 0$ in the middle and right columns of Fig. 2, respectively, the reflections of waves in the corresponding direction are mitigated significantly. The results obtained with the commercial FEM software are not presented for the sake of conciseness. The spatially averaged relative error, defined as $|\mathbf{p} - \mathbf{p}_{FEM}|/|\mathbf{p}|$ with $\mathbf{p}_{FEM}$ the sound pressure vector obtained using the FEM, is less than 0.05% in all cases.

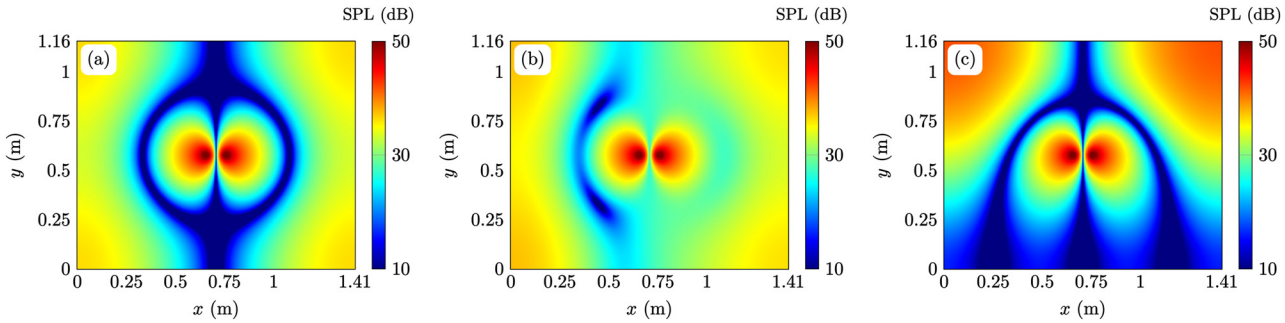

FIG. 2. (Color online) Sound fields at 191 Hz (1,1 mode) generated by a dipole consisting of two point sources located at $(L_x/2 - 0.05\,\mathrm{m}, L_y/2)$ and $(L_x/2 + 0.05\,\mathrm{m}, L_y/2)$ in a 2D rectangular enclosure, where (left) all walls are rigid; (middle) $x = L_x$ is covered with absorptive material; (right) $y = 0$ is covered with absorptive material.

https://doi.org/10.1121/10.0020070

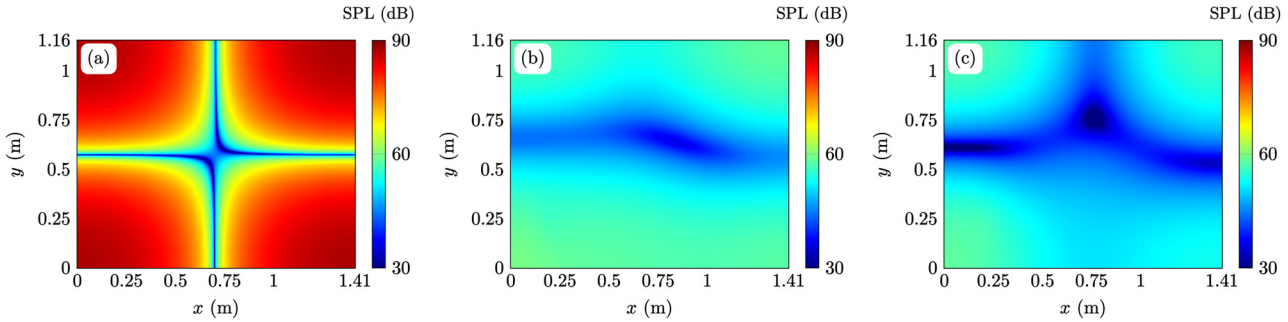

FIG. 3. (Color online) Sound fields at 191 Hz (1,1 mode) generated by a line source in a 2D rectangular enclosure, where (left) all walls are rigid; (middle) $x = L_x$ is covered with absorptive material; (right) $y = 0$ is covered with absorptive material. The source centroid is located at $\boldsymbol{\rho}_c = (0.2\,\text{m}, 0.2\,\text{m})$, and the radiation angle is $\varphi_d = 15^\circ$.

2. Cylindrical harmonic representation of a line source

The second example is a line source with a length of $2a$ placed on the y' axis, which is usually used to simulate a baffled line piston source in 2D models.[39,40] It has a directional beam pattern at large ka due to the aperture effects. The source density can be written as $q'(\boldsymbol{\rho}'_s) = (Q_0/2a)\Pi(y'_s/2a)\delta(x'_s)$,[46] where the denominator $2a$ is to ensure that the line source has a total surface velocity of Q_0, and the rectangle function $\Pi(\zeta) = 1$ when $-1/2 < \zeta < 1/2$, and $\Pi(\zeta) = 0$ otherwise. The cylindrical expansion coefficients are[39,40]

$$A_{2m}(k) = \frac{Q_0}{a}\int_0^a J_{2m}(k\rho'_s)\mathrm{d}\rho'_s, \tag{49}$$

and $A_{2m+1}(k) = 0$, where the integral with respect to J_{2m} can be efficiently evaluated using the Gauss–Legendre quadrature,[39] hypergeometric functions,[40] and Struve functions.[47] The 2D spatial Fourier transform of the source density is

$$\tilde{q}'(\mathbf{k}'_n) = Q_0\mathrm{sinc}(k_{n_y}{}'a). \tag{50}$$

Figure 3 shows the reverberant sound fields obtained using the proposed method and the FEM at 191 Hz (1,1 mode). The centroid of the line source is located at $\boldsymbol{\rho}_c = (0.2\,\text{m}, 0.2\,\text{m})$, and the direction angle is $\varphi_d = 15^\circ$. It can be found from the left column of Fig. 3 that a clear modal pattern is excited when all walls are rigid as the line source is placed close to a corner of the enclosure. The mode in the x and y directions tends to diminish when the wall is absorptive on $x = L_x$ and $y = 0$, as shown in the middle and right columns of Fig. 3, respectively. The spatially averaged relative error against the FEM is less than 0.05%, which validates the accuracy of the proposed method.

To show the reverberant sound field generated by a highly directional source, the SPL at 40 kHz is given in Fig. 4 with other parameters being the same as those used in Fig. 3. This frequency is a typical carrier frequency for the PAL, and there is a need for accurately calculating the reverberant sound fields at this frequency in an enclosure.[46] It can be found in the left column of Fig. 4 that highly directional beams propagate along the radiation axis and experience multiple reflections between walls. The truncation of the directional beam after the incidence on the absorptive wall can be clearly identified in the middle and right columns of Fig. 4. In such a case, the spatially averaged relative error against the FEM is found to be less than 0.8%, which validates the accuracy of the proposed method even at a very high frequency.

B. Directional sources in a 3D enclosure

1. Point monopole source array

In 3D space, supposing an array consisting of N_s point monopole sources with the ith source located at $\mathbf{r}'_{s,i} = (r'_{s,i}, \theta'_{s,i}, \varphi'_{s,i})$ described under the primed coordinate system, the

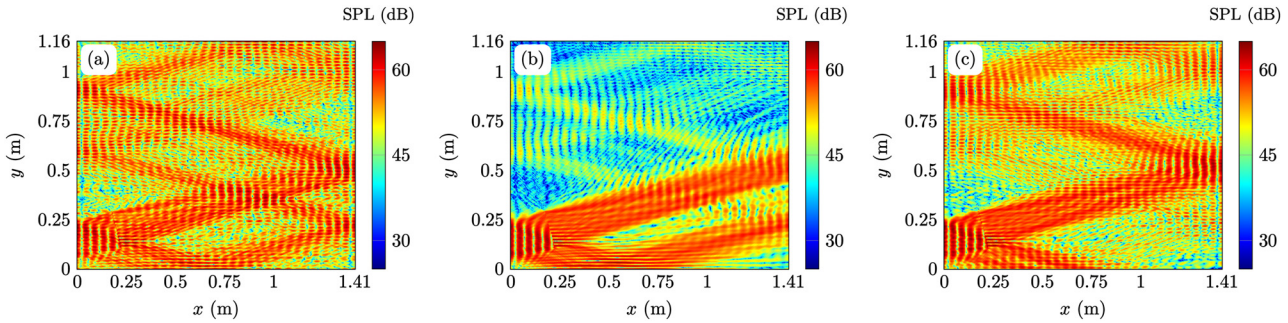

FIG. 4. (Color online) Sound fields at 40 kHz generated by a line source in a 2D rectangular enclosure, where (left) all walls are rigid; (middle) $x = L_x$ is covered with absorptive material; (right) $y = 0$ is covered with absorptive material. The source centroid is located at $\boldsymbol{\rho}_c = (0.2\,\text{m}, 0.2\,\text{m})$, and the radiation angle is $\varphi_d = 15^\circ$.

source density can be described as $q'(\mathbf{r}'_s) = \sum_{i=1}^{N_s} Q_{s,i}\delta(\mathbf{r}'_s - \mathbf{r}'_{s,i})$. The spherical harmonic expansion coefficients can be obtained by using Eqs. (7) and (10) as[8]

$$A_\ell^m(k) = \sum_{i=1}^{N_s} Q_{s,i} j_\ell(kr'_{s,i}) Y_\ell^{m,*}(\theta'_{s,i}, \varphi'_{s,i}). \tag{51}$$

The 3D spatial Fourier transform of the source density is

$$\tilde{q}'(\mathbf{k}'_n) = \sum_{i=1}^{N_s} Q_{s,i} e^{-i\mathbf{k}'_n \cdot \mathbf{r}'_{s,i}}. \tag{52}$$

In this subsection, a simple directional source that generates a dipole outgoing sound field is considered first. The dipole is approximated by two point monopole sources located at $(L_x/2 - 0.05\,\text{m}, L_y/2 - 0.05\,\text{m}, L_z/2 - 0.05\,\text{m})$ and $(L_x/2 + 0.05\,\text{m}, L_y/2 + 0.05\,\text{m}, L_z/2 + 0.05\,\text{m})$ with source strengths of $-Q_0$ and Q_0. Figure 5 presents the SPL in the orthogonal slice planes in the x, y, and z directions with the cross-point at the source centroid, obtained using the proposed method at 223 Hz, which is 1,1,1 mode defined for an enclosure with rigid walls. The spatially averaged relative error against the FEM is found to be less than 0.1%. The figures obtained using the FEM are almost the same as Fig. 5, so they are not presented for conciseness. Similar to the dipole in a 2D rectangular enclosure as shown in Fig. 2, the dipole radiation pattern as well as the effects of the absorptive wall can be clearly observed in Fig. 5.

2. Spherical harmonic representation of a circular source

The second example in the 3D model is a circular source with a radius of a placed on the plane $z' = 0$, which is usually used to simulate a baffled circular piston source.[43,48] It has a directional beam pattern at large ka. The source density can be written as $q'(\mathbf{r}'_s) = (Q_0/\pi a^2)\mathrm{H}(a - \rho'_s)\delta(z'_s)$, where the denominator πa^2 is to ensure that the source has a total volume velocity of Q_0, and $\mathrm{H}(\zeta)$ is the Heaviside function, which is 1 when $\zeta \geq 0$ and 0 when $\zeta < 0$. The spherical expansion coefficients are[43,48]

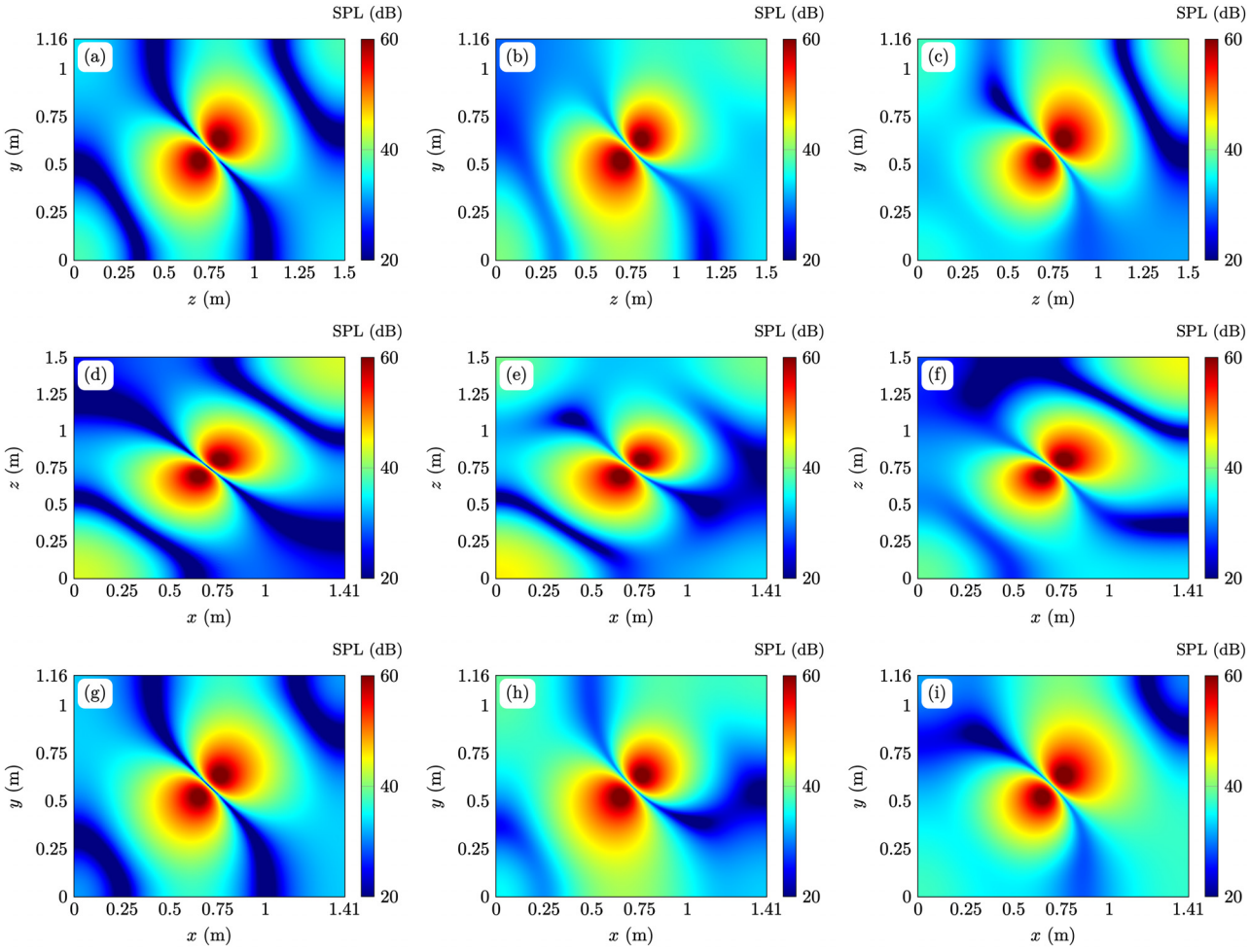

FIG. 5. (Color online) Sound fields at 223 Hz (1,1,1 mode) generated by a dipole in a 3D rectangular enclosure, where (left) all walls are rigid; (middle) $x = L_x$ is covered with absorptive material; (right) $y = 0$ is covered with absorptive material. The source centroid is located at $\mathbf{r}_c = (L_x/2, L_y/2, L_z/2)$, and the coordinates of two point sources are $\mathbf{r}'_{s,1} = (-0.05\,\text{m}, -0.05\,\text{m}, -0.05\,\text{m})$ and $\mathbf{r}'_{s,2} = (0.05\,\text{m}, 0.05\,\text{m}, 0.05\,\text{m})$. Results are obtained in the plane (top) $x = x_c$, (middle) $y = y_c$, or (bottom) $z = z_c$.

https://doi.org/10.1121/10.0020070

$$A_{2\ell}^{m}(k) = \frac{Q_0}{a^2}\delta_{m,0}Y_{2\ell}^{0}(\pi/2, 0)\int_0^a \mathrm{j}_{2\ell}(kr_\mathrm{s})r_\mathrm{s}\mathrm{d}r_\mathrm{s}, \tag{53}$$

and $A_{2\ell+1}^{m}(k) = 0$, where the integral involving $\mathrm{j}_{2\ell}$ can be efficiently evaluated using the Gauss–Legendre quadrature,[43] hypergeometric functions,[48] and closed-form solutions.[49] The 3D spatial Fourier transform of the source density is

$$\tilde{q}'(\mathbf{k}_n') = Q_0\mathrm{jinc}\left(\sqrt{k_{n_x}'^2 + k_{n_y}'^2}a\right), \tag{54}$$

where the jinc function $\mathrm{jinc}(x) \equiv 2J_1(x)/x$.

Figure 6 shows the reverberant sound fields obtained using the proposed method at 223 Hz (1,1,1 mode). The centroid of the circular source is located at $\mathbf{r}_\mathrm{c} = (0.2\,\mathrm{m}, 0.2\,\mathrm{m}, 0.2\,\mathrm{m})$, and the radiation angles are $(\theta_\mathrm{d}, \varphi_\mathrm{d}) = (90^\circ, 15^\circ)$. The modal pattern and the effects of absorptive walls in Fig. 6 are the same as those presented for a 2D enclosure as shown in Fig. 3. The spatially averaged relative error against the FEM is found to be less than 0.04% in this example. Figure 7 shows the reverberant sound fields at 40 kHz with other parameters being the same as those used in Fig. 6. As expected, a highly directional beam is observed, and the major energy of the beam lies in the xOy plane as shown in the bottom row of Fig. 7. The middle and right columns demonstrate the significant effects of absorptive walls. It is noted that our computer is unable to perform the simulation using the FEM for this case because the required memory is too large, and the calculation is very time-consuming. Therefore, the spatially averaged relative error against the FEM is not available for this case.

C. Computation efficiency

In this subsection, the computational efficiency of the proposed method is analyzed based on the numerical results obtained using MATLAB 2022a on a personal computer with an AMD Ryzen™ Threadripper™ 3960X (Santa Clara, CA) central processing unit (CPU) with 256 GB of random access memory (RAM). Table I compares the calculation time to obtain the reverberant sound fields using the direct modal summation, the modal summation with FFT, and the FEM. The calculation time is measured for evaluating the sound pressure at all grid points in the enclosure. The grid

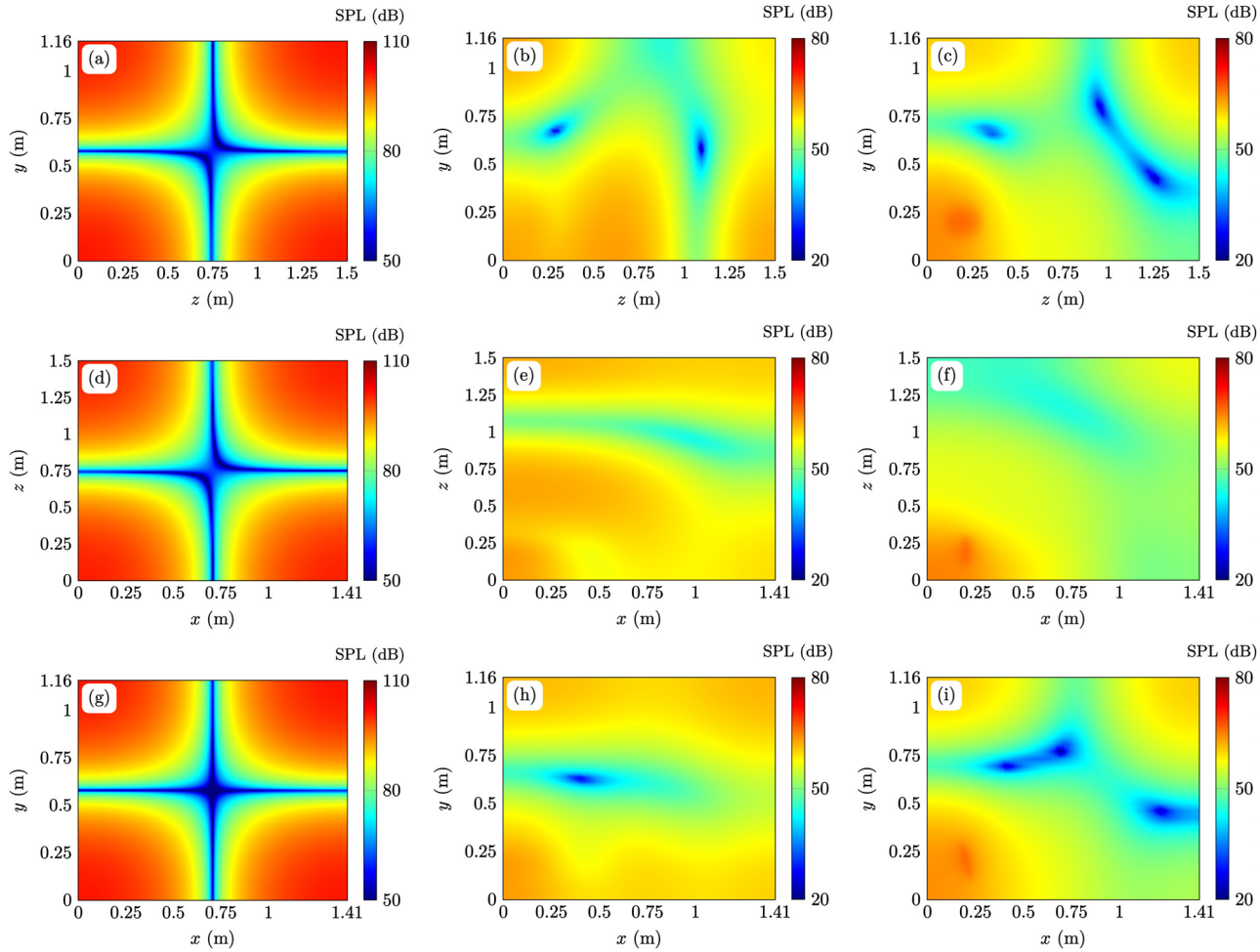

FIG. 6. (Color online) Sound fields at 223 Hz (1,1,1 mode) generated by a circular source in a 3D rectangular enclosure, where (left) all walls are rigid; (middle) $x = L_x$ is covered with absorptive material; (right) $y = 0$ is covered with absorptive material. The source centroid is located at $\mathbf{r}_\mathrm{c} = (0.2\,\mathrm{m}, 0.2\,\mathrm{m}, 0.2\,\mathrm{m})$, and the radiation angles are $(\theta_\mathrm{d}, \varphi_\mathrm{d}) = (90^\circ, 15^\circ)$. Results are obtained in the plane (top) $x = x_\mathrm{c}$, (middle) $y = y_\mathrm{c}$, or (bottom) $z = z_\mathrm{c}$.

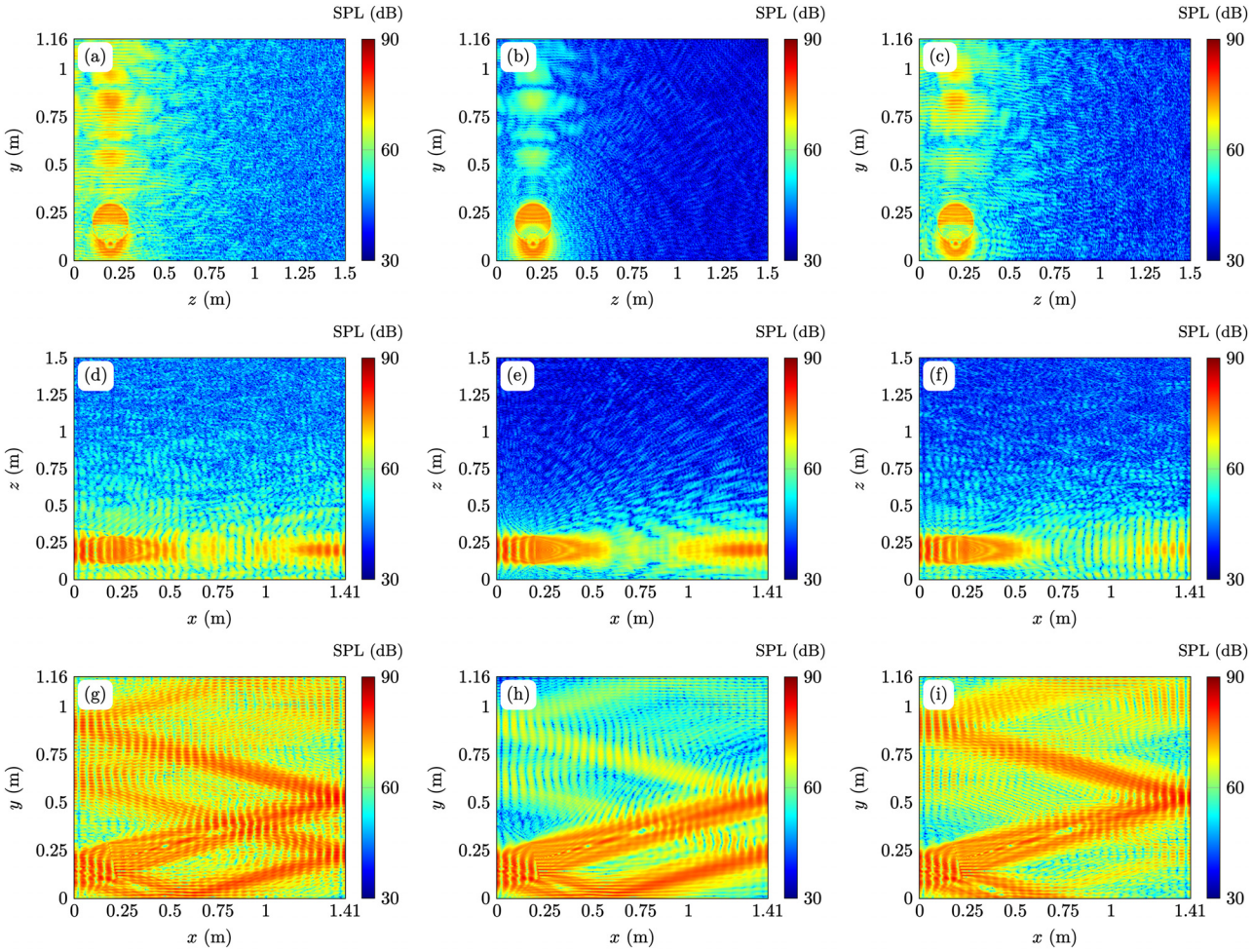

FIG. 7. (Color online) Sound fields at 40 kHz generated by a circular source in a 3D rectangular enclosure, where (left) all walls are rigid; (middle) $x = L_x$ is covered with absorptive material; (right) $y = 0$ is covered with absorptive material. The source centroid is located at $\boldsymbol{\rho}_c = (0.2\,\text{m}, 0.2\,\text{m})$, and the radiation angle is $\varphi_d = 15^\circ$. Results are obtained in the plane (top) $x = x_c$, (middle) $y = y_c$, or (bottom) $z = z_c$.

points in x, y, and z directions are 35, 30, and 35, respectively, at 191 and 223 Hz. At 40 kHz, the grid points in x, y, and z directions are 350, 300, and 350, respectively. It is noted that the exact calculation time is not presented for the FEM at 40 kHz in the 3D enclosure because the calculation is very time-consuming. Our simulations showed that the elapsed time for this case is at least more than 2 h (7200 s). It can be found that the FEM can obtain converged results with an acceptable calculation time at low frequencies, but it becomes very time-consuming at high frequencies. The MEM consistently exhibits superior computational efficiency in all cases, and its performance can be further enhanced through the utilization of the FFT. When all walls are rigid, the proposed modal summation with FFT method can be more than 100 times faster than the FEM. The improvement of the computation efficiency of the proposed method deteriorates when one wall is absorptive because the FFT cannot be used in the direction perpendicular to this wall as discussed in Sec. III D. However, the proposed method is still much more efficient than the FEM and, thus, provides an alternative to simulating reverberant sound fields even in a large room and/or at high frequencies.

TABLE I. Calculation time of the MEM and the FEM.

	Frequency	Modal summation using FFT (s)	Direct modal summation (s)	FEM (s)
2D enclosure with rigid walls	191 Hz	0.05	0.81	2
	40 kHz	0.07	1.38	244
2D enclosure with one absorptive wall	191 Hz	0.25	1.02	3
	40 kHz	0.36	2.21	271
3D enclosure with rigid walls	223 Hz	0.13	13.22	22
	40 kHz	81	3302	>7200
3D enclosure with one absorptive wall	223 Hz	0.75	15.1	34
	40 kHz	243	3811	>7200

VI. CONCLUSIONS

This paper developed a wave-based simulation method for calculating the non-diffuse reverberant sound field generated by a directional source in both 2D and 3D rectangular enclosures using the modal expansions. This work may find its application in investigating the reverberation effects of directional sources on sound field reproductions, active

https://doi.org/10.1121/10.0020070

noise control systems, and so on. The idea of the proposed method is to express the modal source density using the cylindrical or spherical harmonic expansion coefficients of the directional source. The numerical results with several typical directional sources are presented, and the accuracy is validated by the comparison against those obtained using the FEM. To improve the computation efficiency, the summation of enclosure modes was written in the form of discrete Fourier transform so that the FFT can be used for lightly damped or rigid walls. This makes it possible to obtain accurate reverberant sound fields at a high frequency even up to 40 kHz with a relatively low computational load. It is noted that the computation of the modal summation via FFT is more efficient if the responses at a large number of receivers are required. This technique is, therefore, useful for the field visualization and walk-through auralization. In some applications in room acoustics, other physical fields, including the particle velocity and the sound intensity, are also required, and their calculations using the proposed method are a straightforward extension of the presented approach. The sources are increasingly measured via cylindrical or spherical harmonics.[17] In future work, we aim to validate the measured cylindrical and spherical harmonics for specific sources through experimental verification.

ACKNOWLEDGMENTS

The authors would like to thank Dr. Chengbo Hu and Lei Gu for advice with the FEM simulations. H.Z. and J.L. gratefully acknowledge financial support by the National Natural Science Foundation of China (Grant No. 12274221).

[1]N. Tanaka and M. Tanaka, "Active noise control using a steerable parametric array loudspeaker," J. Acoust. Soc. Am. **127**(6), 3526–3537 (2010).
[2]J. Zhong, T. Zhuang, R. Kirby, M. Karimi, H. Zou, and X. Qiu, "Quiet zone generation in an acoustic free field using multiple parametric array loudspeakers," J. Acoust. Soc. Am. **151**(2), 1235–1245 (2022).
[3]M. A. Poletti, T. D. Abhayapala, and P. Samarasinghe, "Interior and exterior sound field control using two dimensional higher-order variable-directivity sources," J. Acoust. Soc. Am. **131**(5), 3814–3823 (2012).
[4]T. Betlehem and M. Poletti, "Sound field of a directional source in a reverberant room," N. Z. Acoust. **25**(4), 12–22 (2012).
[5]M. A. Poletti, T. Betlehem, and T. Abhayapala, "Higher-order loudspeakers and active compensation for improved 2D sound field reproduction in rooms," J. Audio Eng. Soc. **63**(1/2), 31–45 (2015).
[6]J. A. Hargreaves, L. R. Rendell, and Y. W. Lam, "A framework for auralization of boundary element method simulations including source and receiver directivity," J. Acoust. Soc. Am. **145**(4), 2625–2637 (2019).
[7]S. Bilbao, J. Ahrens, and B. Hamilton, "Incorporating source directivity in wave-based virtual acoustics: Time-domain models and fitting to measured data," J. Acoust. Soc. Am. **146**(4), 2692–2703 (2019).
[8]P. N. Samarasinghe, T. D. Abhayapala, Y. Lu, H. Chen, and G. Dickins, "Spherical harmonics based generalized image source method for simulating room acoustics," J. Acoust. Soc. Am. **144**(3), 1381–1391 (2018).
[9]M. Nolan and J. L. Davy, "Two definitions of the inner product of modes and their use in calculating non-diffuse reverberant sound fields," J. Acoust. Soc. Am. **145**(6), 3330–3340 (2019).
[10]D. Raudales, D. B. Bliss, K. A. Michalis, J. W. Rouse, and L. P. Franzoni, "Benchmark analytical solutions for steady state high frequency broadband sound fields in three rectangular enclosures," J. Acoust. Soc. Am. **145**(4), 2601–2612 (2019).
[11]J. Poblet-Puig and A. Rodríguez-Ferran, "Modal-based prediction of sound transmission through slits and openings between rooms," J. Sound Vib. **332**(5), 1265–1287 (2013).
[12]S. Wang, Z. Yang, J. Tao, X. Qiu, and I. S. Burnett, "Transmission loss and directivity of sound transmitted through a slit on ground," J. Acoust. Soc. Am. **153**(1), 224–235 (2023).
[13]S. Wang, J. Tao, and X. Qiu, "Performance of a planar virtual sound barrier at the baffled opening of a rectangular cavity," J. Acoust. Soc. Am. **138**(5), 2836–2847 (2015).
[14]Y. Y. Li and L. Cheng, "Modifications of acoustic modes and coupling due to a leaning wall in a rectangular cavity," J. Acoust. Soc. Am. **116**(6), 3312–3318 (2004).
[15]J. Escolano, J. J. López, and B. Pueo, "Directive sources in acoustic discrete-time domain simulations based on directivity diagrams," J. Acoust. Soc. Am. **121**(6), EL256–EL262 (2007).
[16]D. T. Murphy, A. Southern, and L. Savioja, "Source excitation strategies for obtaining impulse responses in finite difference time domain room acoustics simulation," Appl. Acoust. **82**, 6–14 (2014).
[17]W. Klippel and C. Bellmann, "Holographic nearfield measurement of loudspeaker directivity," in *Proceedings of Audio Engineering Society Convention 141*, Los Angeles, CA (September 29–October 2, 2016).
[18]M. A. Poletti, "Three-dimensional surround sound systems based on spherical harmonics," J. Audio Eng. Soc. **53**(11), 1004–1025 (2005).
[19]H. Kuttruff, *Room Acoustics*, 6th ed. (CRC, Boca Raton, FL, 2017).
[20]L. Savioja and U. P. Svensson, "Overview of geometrical room acoustic modeling techniques," J. Acoust. Soc. Am. **138**(2), 708–730 (2015).
[21]J. B. Allen and D. A. Berkley, "Image method for efficiently simulating small-room acoustics," J. Acoust. Soc. Am. **65**(4), 943–950 (1979).
[22]S. G. McGovern, "Fast image method for impulse response calculations of box-shaped rooms," Appl. Acoust. **70**(1), 182–189 (2009).
[23]W. Zhang, P. N. Samarasinghe, and T. D. Abhayapala, "Parameterization of the binaural room transfer function using modal decomposition," J. Acoust. Soc. Am. **146**(1), EL8–EL14 (2019).
[24]L. Birnie, T. D. Abhayapala, H. Chen, and P. N. Samarasinghe, "Sound source localization in a reverberant room using harmonic based music," in *Proceedings of ICASSP 2019—2019 IEEE International Conference on Acoustics, Speech and Signal Processing (ICASSP)*, Brighton, UK (May 12–17, 2019), pp. 651–655.
[25]L. I. Birnie, T. D. Abhayapala, and P. N. Samarasinghe, "Reflection assisted sound source localization through a harmonic domain MUSIC framework," IEEE/ACM Trans. Audio Speech Lang. Process. **28**, 279–293 (2020).
[26]N. Murata, J. Zhang, Y. Maeno, and Y. Mitsufuji, "Global and local mode-domain adaptive algorithms for spatial active noise control using higher-order sources," in *Proceedings of CASSP 2019–2019 IEEE International Conference on Acoustics, Speech and Signal Processing (ICASSP)*, Brighton, UK (May 12–17, 2019), pp. 526–530.
[27]H. Sun, T. D. Abhayapala, and P. N. Samarasinghe, "A realistic multiple circular array system for active noise control over 3D space," IEEE/ACM Trans. Audio Speech Lang. Process. **28**, 3041–3052 (2020).
[28]T. Betlehem and M. A. Poletti, "Two dimensional sound field reproduction using higher order sources to exploit room reflections," J. Acoust. Soc. Am. **135**(4), 1820–1833 (2014).
[29]H. Zuo, T. D. Abhayapala, and P. N. Samarasinghe, "Particle velocity assisted three dimensional sound field reproduction using a modal-domain approach," IEEE/ACM Trans. Audio Speech Lang. Process. **28**, 2119–2133 (2020).
[30]M. Aretz, P. Dietrich, and M. Vorländer, "Application of the mirror source method for low frequency sound prediction in rectangular rooms," Acta Acust. united Acust. **100**(2), 306–319 (2014).
[31]E. A. Lehmann and A. M. Johansson, "Prediction of energy decay in room impulse responses simulated with an image-source model," J. Acoust. Soc. Am. **124**(1), 269–277 (2008).
[32]R. Duraiswami, D. N. Zotkin, and N. A. Gumerov, "Fast evaluation of the room transfer function using multipole expansion," IEEE Trans. Audio Speech Lang. Process. **15**(2), 565–576 (2007).
[33]P. M. Morse and R. H. Bolt, "Sound waves in rooms," Rev. Mod. Phys. **16**(2), 69–150 (1944).
[34]J. T. Du, W. L. Li, Z. G. Liu, H. A. Xu, and Z. L. Ji, "Acoustic analysis of a rectangular cavity with general impedance boundary conditions," J. Acoust. Soc. Am. **130**(2), 807–817 (2011).

[35]B. Xu and S. D. Sommerfeldt, "A hybrid modal analysis for enclosed sound fields," J. Acoust. Soc. Am. **128**(5), 2857–2867 (2010).
[36]M. Meissner, "Acoustic behaviour of lightly damped rooms," Acta Acust. united Acust. **99**, 845–847 (2013).
[37]ISO 9613-1:1993, "Acoustics—Attenuation of sound during propagation outdoors—Part 1: Calculation of the absorption of sound by the atmosphere" (International Organization for Standardization, Geneva, Switzerland, 1993).
[38]T. Betlehem and T. D. Abhayapala, "Theory and design of sound field reproduction in reverberant rooms," J. Acoust. Soc. Am. **117**(4), 2100–2111 (2005).
[39]J. Zhong, R. Kirby, M. Karimi, and H. Zou, "A cylindrical expansion of the audio sound for a steerable parametric array loudspeaker," J. Acoust. Soc. Am. **150**(5), 3797–3806 (2021).
[40]M. A. Poletti, "Cylindrical expansions of sound radiation from resilient and rigid infinite strips with reduced error," J. Acoust. Soc. Am. **145**(5), 3104–3115 (2019).
[41]E. G. Williams, *Fourier Acoustics: Sound Radiation and Nearfield Acoustical Holography* (Academic, San Diego, CA, 1999).
[42]I. Ben Hagai, M. Pollow, M. Vorländer, and B. Rafaely, "Acoustic centering of sources measured by surrounding spherical microphone arrays," J. Acoust. Soc. Am. **130**(4), 2003–2015 (2011).
[43]J. Zhong, R. Kirby, and X. Qiu, "A spherical expansion for audio sounds generated by a circular parametric array loudspeaker," J. Acoust. Soc. Am. **147**(5), 3502–3510 (2020).
[44]Y. Naka, A. A. Oberai, and B. G. Shinn-Cunningham, "Acoustic eigenvalues of rectangular rooms with arbitrary wall impedances using the interval Newton/generalized bisection method," J. Acoust. Soc. Am. **118**(6), 3662–3671 (2005).
[45]H.-C. Shin, "Time-harmonic convention of exp(–$i\omega t$) can be preferable to exp(+$i\omega t$)(L)," J. Acoust. Soc. Am. **146**(3), 1851–1854 (2019).
[46]J. Zhong, R. Kirby, M. Karimi, X. Qiu, and J. Lu, "Audio sound field generated by a parametric array loudspeaker in a rectangular room with lightly damped walls," in *Proceedings of the 24th International Congress on Acoustics*, Gyeongju, Korea (October 24–28, 2022).
[47]W. Rosenheinrich, "Tables of some indefinite integral of Bessel functions of integer order," https://www.eah-jena.de/fileadmin/user_upload/eah-jena.de/fachbereich/gw/Ehemalige/rosenheinrich/Rosenheinrich_2011_2012_2021.pdf (Last viewed June 30, 2023).
[48]M. A. Poletti, "Spherical expansions of sound radiation from resilient and rigid disks with reduced error," J. Acoust. Soc. Am. **144**(3), 1180–1189 (2018).
[49]J. Zhong and X. Qiu, "On the spherical expansion for calculating the sound radiated by a baffled circular piston," J. Theor. Comp. Acoust. **28**, 2050026 (2020).